2-Aminopurine Electronic Structure and Fluorescence Properties in DNA†

John M. Jean* and Kathleen B. Hall

Department of Biochemistry and Molecular Biophysics, Washington University School of Medicine, St Louis, Missouri 63110

Received April 24, 2002

ABSTRACT: 2-Aminopurine (2AP) fluorescence intensity and decay lifetimes have been used as indicators of nucleic acid geometry and dynamics. To characterize 2AP photophysics in the context of a DNA strand, time-dependent density functional theory is applied to 2AP stacked with two flanking nucleobases. Calculations show that 2AP in the trimers suffers a reduction in the oscillator strength of its low-lying $\pi-\pi^*$ 2AP-like allowed transition, manifested in a reduction of its radiative rate. Trimers also exhibit two or three lower-energy excited states (charge transfer states) that are predicted to facilitate nonradiative transitions from the fluorescent excited state.

The fluorescent adenine isomer, 2-aminopurine (2AP),[1] is widely employed as a reporter of the structure and dynamics of nucleic acids because of its ability to form Watson−Crick base pairs with thymine (uracil); its red-shifted absorption maximum, which allows for selective excitation; and the sensitivity of its fluorescence properties to structural context. 2AP fluorescence is strongly quenched in both single- and double-stranded DNA (*1*), and this property has been exploited to probe the dynamics of melting (*2*, *3*), abasic sites (*4*, *5*), mismatched base pairs (*6*), and metal ion binding (*4*, *7*) as well as the thermodynamics and kinetics of protein-induced DNA conformational transitions (*8*−*15*). The fluorescence decay of 2AP in nucleic acids is highly nonexponential, with components typically ranging from 10 ps to 10 ns (*2*, *5*, *6*) that have been interpreted to reflect a distribution of local conformations in which 2AP experiences varying degrees of stacking.

Interpretation of 2AP fluorescence in terms of its local environment requires identification of quenching mechanisms and their dependence on sequence and structural contexts. Charge transfer (CT) processes have recently been invoked as mechanisms of quenching of 2AP fluorescence (*16*−*19*). Hole transfer and electron transfer are complementary CT processes. In the former, an electron vacancy moves to a site with a lower ionization potential (guanine has the lowest ionization potential of the nucleobases); in the latter, an electron moves to a site of higher electron affinity (thymine has the highest electron affinity of the nucleobases). Recently, Larsen et al. (*16*) used picosecond fluorescence lifetime and polarization measurements to probe the dynamics of a DNA hairpin in which individual adenines were replaced with 2AP. In each structure, they observed large amplitude decay components with time constants ranging from ∼10 to 20 ps, which they assigned to hole transfer from excited 2AP to guanosine. Kelley and Barton (*17*) showed that photoexcited 2AP oxidizes guanosine and used the resultant fluorescence quench to monitor hole transport kinetics in a series of DNA duplexes. Zewail and co-workers investigated the sequence dependence of charge transfer processes involving excited 2AP in duplex DNA using femtosecond transient absorption (*18*). Their results showed that all bases can undergo charge transfer with photoexcited 2AP when located on its 3′ side. On the basis of the dependence of the rate of charge transfer on the thermodynamic driving force, these authors suggest that the 2AP excited state decays by hole transfer to neighboring purines, or by electron transfer to neighboring pyrimidines.

Mechanisms in addition to charge transfer may also contribute to 2AP quenching. Rachofsky et al. (*20*) have shown that the 2AP lifetime decreases with decreasing solvent polarity, which could be responsible, in part, for the short components of 2AP in DNA, since different local conformations would experience different polarities. However, even in nonpolar solvents, such as dioxane, the lifetime was found to be ∼1−2 ns, considerably longer than the sub-nanosecond decay components that are ubiquitous in 2AP-labeled DNAs.

Establishing the nature of the molecular interactions that lead to fluorescence quenching of 2AP in DNA is critical for the accurate interpretation of experimental fluorescence data in terms of structure and dynamics. The electronic structure of 2AP is the key to understanding how this nucleobase is influenced by solvent electrostatics, hydrogen bonding, and aromatic π-stacking interactions. Excited state CIS calculations on 2AP assigned the $S_0 \rightarrow S_1$ and $S_0 \rightarrow S_2$ transitions as $\pi-\pi^*$ and $n-\pi^*$ transitions, respectively (*21*−*23*), in agreement with experiment (*24*), and yielded a value for the $S_0 \rightarrow S_1$ transition dipole direction in good agreement with that obtained from linear dichroism experiments of 2AP in oriented PVA films (*24*). The oscillator strengths and excitation energies, however, were substantially overestimated due to the inability of CIS to accurately handle dynamic electron correlation effects. Recently, Rachofsky et al. carried out multiconfigurational CASSCF-based cal-

† This work was supported by ACS Petroleum Research Fund Grant 36506-AC6 (J.M.J.) and by the National Science Foundation (K.B.H.).

[1] Abbreviations: 2AP, 2-aminopurine; TDDFT, time-dependent density functional theory; CASSCF, complete active subspace self-consistent field; CIS, configuration interaction singles; HOMO, highest occupied molecular orbital; LUMO, lowest unoccupied molecular orbital.

10.1021/bi020308y CCC: $22.00
Published on Web 10/09/2002

culations of 2-amino-9-methylpurine (*25*), which provide a much better treatment of electron correlation and thus more accurate values for excitation energies. Using a dielectric continuum (Onsager cavity) model to treat electrostatic solvent effects and the computed permanent dipole moments of the ground and excited states, they find that the $\pi-\pi^*$ to $n-\pi^*$ energy gap decreases with decreasing solvent polarity. They propose that a solvent-mediated vibronic coupling between these two states could account for the reduction of the 2AP lifetime in nonpolar environments.

Our recent work has attempted to understand the influence of π-stacking interactions on the excited state transitions of 2AP using time-dependent density functional theory (TDDFT). Previously, we reported excitation energies, oscillator strengths, and transition dipole directions for the four native bases and 2AP alone and in $^{5'}$2AP$-$X$^{3'}$ (X is A, T, G, or C) and $^{5'}$T$-$2AP$^{3'}$ dimers with canonical B-form geometry (*19*). For individual bases, TDDFT results for electronic state ordering and excitation energies were found to be in excellent agreement with the results from experiments. For isolated 2AP, we found the $\pi-\pi^*$ and $n-\pi^*$ transitions occur at 292 and 275 nm, respectively, compared to the experimental values of 305 and 278 nm, respectively, which were obtained in polar media. The oscillator strength for the $S_0 \rightarrow S_1$ transition was computed to be 0.127 compared to the experimental value of 0.10. These results represent a considerable improvement in accuracy over CIS and are comparable to those obtained by the more computationally intensive CASSCF method. The dimer calculations showed that π-stacking interactions lead to the formation of states with substantial charge transfer (CT) character and provided a qualitative theoretical explanation for quenching observed for 2AP.

The dimer results pertain most immediately to cases where a DNA is labeled with 2AP at the 5′ end. In many experimental studies, the 2AP is stacked on both the 5′ and 3′ sides; hence, we have extended our work to investigate the optical properties and photophysical pathways of 2AP-containing trimers. Here, we report TDDFT results where 2AP is flanked by guanines (purine) and/or thymines (pyrimidine), forming a $^{5'}$X$-$2AP$-$Y$^{3'}$ sandwich of nucleobases. On the basis of current and previous results with $^{5'}$X$-$2AP$^{3'}$ and $^{5'}$2AP$-$Y$^{3'}$ dimers, we describe the extent to which the trimer can be constructed from dimer combinations.

COMPUTATIONAL METHODS

Density functional theory (DFT) has become widely used in the study of molecular electronic structure during the past decade due to its computational efficiency and its success in calculating a wide range of ground state properties. In DFT, the ground state electron density (rather than the wave function) is treated variationally (*26*). Exchange and correlation effects are incorporated through an exchange-correlation functional. The usual implementation of DFT for quantum chemical problems involves the iterative solution of the Kohn$-$Sham equation (*26*, *27*), which produces a set of one-electron molecular (KS) orbitals optimized to give a noninteracting electron density equal to the "true" density. The recent extension of DFT to the time domain (TDDFT) allows the calculation of the linear response of this ground state density to a time-dependent external electric potential, $\delta v(t)$ (*28*$-$*30*). In the frequency domain, the change in density is given by

$$\delta\rho(r,\omega) = \sum_{ai}\delta P_{ai}(\omega)\varphi_a(r)\varphi^*_i(r) + \sum_{ia}\delta P_{ai}(\omega)\varphi_i(r)\varphi^*_a(r)$$

where a refers to occupied molecular orbitals (MOs) and i to unoccupied MOs. $\delta P(\omega)$ is the response of the density matrix in the supermolecule MO (Ψ_i) basis. Transition energies and transition dipole moments are then obtained from the poles and residues of the density$-$density response function, $\chi(r,r',\omega)$, which relates the change in the electron density to the external field.

$$\delta\rho(r,\omega) = \int dr'\, \chi(r,r',\omega)\, \delta v(r',\omega)$$

Calculations were performed using Gaussian 98 (*31*) and the molecular orbitals rendered using the program Molden (*32*). The implementation of TDDFT in Gaussian 98 makes use of the adiabatic approximation (*30*). All reported results were obtained using the triple-ζ 6-311+G(d) basis with the hybrid B3LYP exchange-correlation functional (*33*), which has been shown to provide accurate values for low-lying valence transition energies for a wide range of molecules (*19*, *30*, *34*, *35*). This class of functionals has also been shown to provide the most accurate results for ground state CT complexes (*36*). Excitation energies and oscillator strengths obtained using other hybrid functionals (B3PW91) were found to agree to within ~3% with those obtained using B3LYP. Calculations carried out on 2AP at the 6-311+G(d) level using the local density approximation (LDA) yielded a $\pi-\pi^*$ transition of 319 nm, in close agreement with the experimental value; however, the $n-\pi^*$ transition was predicted to have a transition wavelength of 315 nm compared to the experimental value of 278 nm.

Basis sets with diffuse functions were found to give rise to one or more low-lying excited states with a high degree of Rydberg character, which are not reported in our results. Larger basis sets, which included polarization functions on the hydrogens and/or an extra set of diffuse functions, gave virtually identical results for all electronic properties of the monomers, and selected trimers.

Trimers containing 2AP were generated in INSIGHT II (*37*) from canonical B-form X-ray crystallographic data by mutating adenine to 2AP and removing the sugar and phosphate atoms. The latter step is justified given that the transitions of interest take place between MOs that are localized on the bases. The internal coordinates of each base were optimized separately at the MP2/6-31G(d,p) level, maintaining the helical parameters of the B-form trimer. Geometrically distorted 2AP-containing dimers were obtained in an analogous way; however, before the optimization step, rotations of 2AP about the ζ backbone (O3′$-$P) torsion toward the major groove were made in INSIGHT to generate structures designed to approximate those partially stacked structures that occur transiently during base pair openings in duplex DNA.

Since we are interested in comparing the excited state properties of dimers and trimers with those of the constituent monomers, care must be taken to avoid basis set superposition errors (BSSEs), which may arise from the use of a different number of basis functions for monomers and the

assemblies. These errors were assessed using the Counterpoise method (*38*); transition energies and transition dipole moments were computed for each monomer and compared with trimer (dimer) calculations where all atoms except those of the base of interest were replaced with "ghost" atoms (no nuclear charge or electrons, but the full complement of basis functions) to effectively calculate monomer properties as they would appear in the assembly. Comparison of these results with those from the isolated monomers and selected dimers and trimers showed that the BSSE was <1% for energies, oscillator strengths, and transition dipole directions.

RESULTS

We adopt a "supermolecule" approach, in which the dimer or trimer construct effectively is treated as a single entity (*19*, *39*, *40*). In this method, the molecular orbitals (MOs) of the assembly are generated from a localized atomic orbital basis. More specifically, excited state transitions of the dimer or trimer are expressed as linear combinations of one-electron promotions between occupied and unoccupied supermolecule MOs. Baerends et al. (*40*) have carried out similar TDDFT studies to calculate the optical spectra and hyperpolarizability of porphyrin "sandwich" dimers.

To qualitatively characterize the excited state transitions, the localized (monomer) orbital (LO) picture is useful, in which transitions are described as linear combinations of localized (excitonic) and intermolecular (charge transfer) transitions. In each of the systems reported here, we focus only on those singlet transitions that occur at sufficiently low energy (E < 4.5 eV; λ > 275 nm) to influence the photophysical behavior of 2AP-labeled DNA following excitation under typical experimental conditions.

2-Aminopurine Flanked by Thymines. Previous TDDFT calculations of stacking interactions between 2AP and thymine and cytosine, whether a $^{5'}$2AP−X$^{3'}$ or $^{5'}$X−2AP$^{3'}$ dimer, showed that the electronic effects of the pyrimidines are nearly identical (*19*). While noting that thymine has the higher electron affinity, we use it here as a model system to represent pyrimidines.

$^{5'}$T−2AP−T$^{3'}$ Trimer. To appreciate the electronic structure of the trimer, first the dimers must be considered as components of the larger supermolecule construct. TDDFT calculations show that 2AP−pyrimidine dimers exhibit two transitions in the region above 275 nm. These results can be seen in Figure 1a for the $^{5'}$2AP−T$^{3'}$ dimer. The $S_0 \rightarrow S_2$ transition has a transition wavelength (296 nm) and oscillator strength (0.094) closely resembling those of the isolated 2AP $S_0 \rightarrow S_1$ transition; this transition for the $^{5'}$T−2AP$^{3'}$ dimer is similar (Figure 1b). An additional $S_0 \rightarrow S_1$ transition is present in the dimers that is not seen in the monomers. Each unique dimer transition has a considerably smaller oscillator strength than the $S_0 \rightarrow S_2$ transition; the asymmetry of 5′ and 3′ stacking interactions results in significantly different energies, however (307 and 331 nm, respectively).

The electronic structure of the $^{5'}$T−2AP−T$^{3'}$ trimer, shown in Figure 1c, appears to be a composite of the two dimers because it exhibits three transitions in the region of interest. The $S_0 \rightarrow S_3$ transition has a transition wavelength nearly identical to that of the isolated 2AP $\pi-\pi^*$ transition. The reduction in the oscillator strength of this transition indicates that there is a slightly larger hypochromic effect for the 2AP-like transition in the trimer than in the dimer. The only substantive difference between the excited states of the $^{5'}$T−2AP−T$^{3'}$ trimer and those of either of its dimer fragments is the presence of two states below the dipole-allowed 2AP-like state. On the basis of the relative energies of dimer S_1 states, the S_1 trimer state corresponds to the $S_0 \rightarrow S_1$ transition of the $^{5'}$2AP−T$^{3'}$ dimer, while the S_2 state corresponds to the $S_0 \rightarrow S_1$ transition of the $^{5'}$T−2AP$^{3'}$ dimer.

The above description of the dimer and trimer transitions corresponds to the phenomenological experimental observables. To appreciate the molecular origins of the transitions, however, we examine the dominant one-electron contributions to each electronic transition as determined by the solution vectors (*30*). As illustrated in Figure 1, TDDFT calculations show that the two lowest-lying transitions of a 2AP−pyrimidine dimer receive contributions primarily from one-electron promotions between the highest occupied molecular orbital (HOMO) and the lowest unoccupied molecular orbital (LUMO) and LUMO+1. The 2AP HOMO is much higher in energy (∼1 eV) than that of thymine, so the supermolecule HOMOs are highly localized on the 2AP. The two lowest unoccupied orbitals of the dimers, particularly those of the $^{5'}$2AP−T$^{3'}$ dimer, are delocalized over both bases. These results can be seen in Figure 1a for the $^{5'}$2AP−T$^{3'}$ dimer. The $S_0 \rightarrow S_2$ (70% HOMO → LUMO+1) transition is highly localized on the 2AP and resembles the isolated 2AP $S_0 \rightarrow S_1$ ($\pi-\pi^*$) transition (*19*); this transition for the $^{5'}$T−2AP$^{3'}$ dimer is similar (Figure 1b). Also shown are the orbital populations for the dominant electronic configurations for each excited state. The slight reduction in oscillator strength (and concomitant increase in radiative lifetime) from that of the 2AP $S_0 \rightarrow S_1$ transition arises from the weak contribution of the HOMO → LUMO configuration to this transition. In both dimers, the $S_0 \rightarrow S_1$ (predominantly HOMO → LUMO) transition is seen to result in a shift in electron density from 2AP to thymine, which defines this as a charge transfer (CT) state. In the LO picture, this $S_2 \rightarrow S_1$ transition is described as electron transfer from 2AP to T resulting in formation of the radical cation−radical anion pair.

The electronic structure of the $^{5'}$T−2AP−T$^{3'}$ trimer, shown in Figure 1c, is a composite of the two dimers, in that its three lowest singlet transitions resemble dimer transitions. The $S_0 \rightarrow S_3$ transition is dominated by HOMO → LUMO and HOMO → LUMO+2 transitions (each of which involves partial transfer of electron density to the $^{3'}$T). The orbital contributions in Figure 1 show definitively that the S_1 trimer state corresponds to the S_1 state of the $^{5'}$2AP−T$^{3'}$ dimer, while the S_2 state corresponds to the S_1 state of the $^{5'}$T−2AP$^{3'}$ dimer. The electronic structure of this trimer can be considered a simple superposition of the electronic structures of its dimer fragments, suggesting that the effects of the 5′ and 3′ stacking interactions are relatively independent of one another.

2-Aminopurine Flanked by Guanines. Previous TDDFT calculations for 2AP dimers containing guanine or adenine gave qualitatively similar results. Again noting that guanine has the lowest ionization potential among the bases, we used it here to model 2AP−purine interactions.

In B-form geometry, base overlap between adjacent purines is more extensive than for purine−pyrimidine pairs, and so electronic states of the 2AP−purine dimers and

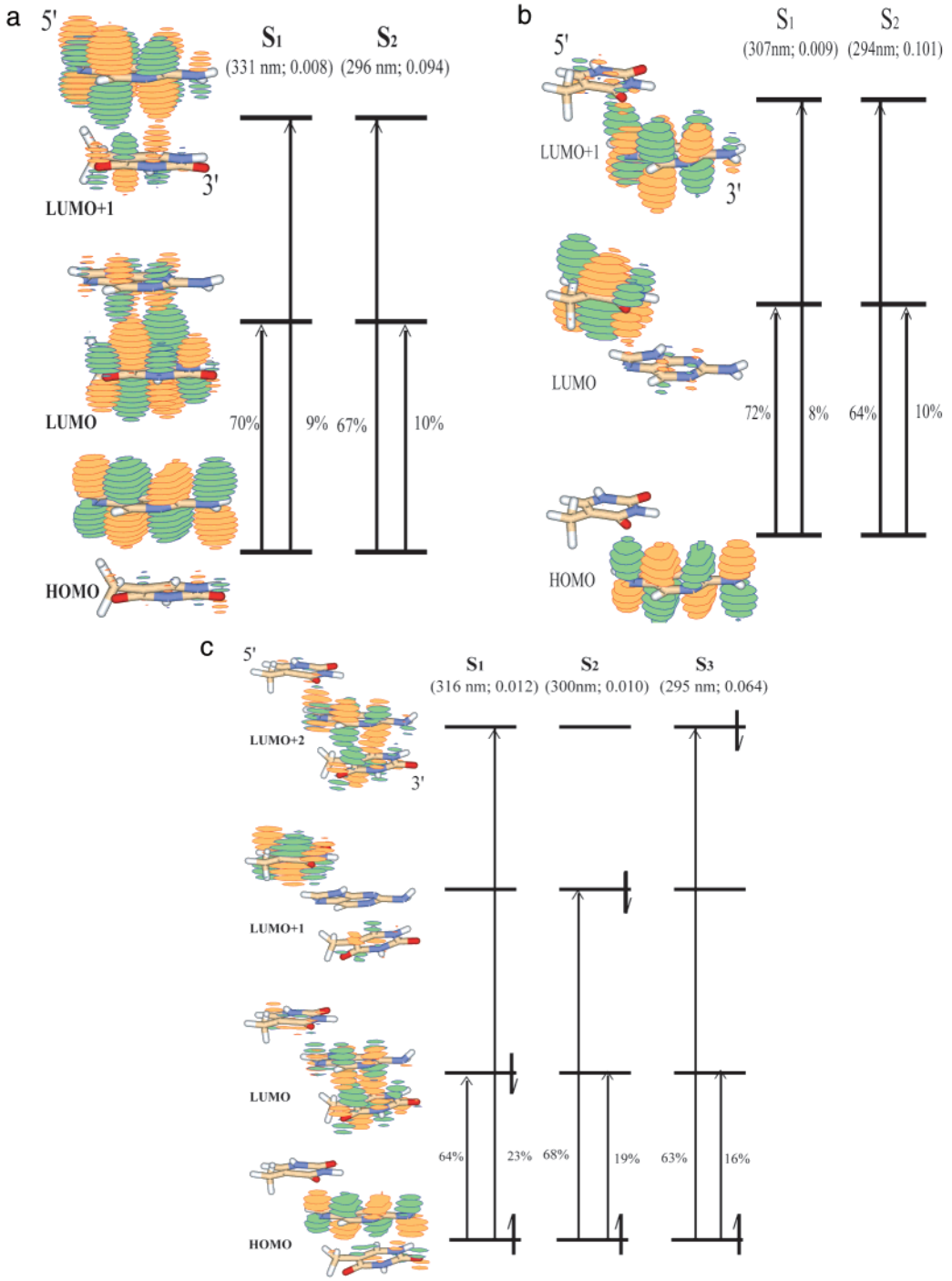

FIGURE 1: Transition wavelengths, oscillator strengths, and one-electron contributions (>10%) for the low-lying excited singlet transitions for systems with 2AP stacked with thymine: (a) $^{5'}$2AP−T$^{3'}$, (b) $^{5'}$T−2AP$^{3'}$, and (c) $^{5'}$T−2AP−T$^{3'}$. In panel c, the electron configuration for the dominant one-electron contribution to each excited state transition is shown.

trimers are expected to reflect this increased overlap of their π-systems. TDDFT calculations for the $^{5'}$2AP−G$^{3'}$ and $^{5'}$G−2AP$^{3'}$ dimers are shown in Figure 2a,b. In the $^{5'}$2AP−G$^{3'}$ dimer, the $S_0 \rightarrow S_1$ and $S_0 \rightarrow S_2$ transitions have oscillator strengths that are approximately half of that of the 2AP ($\pi-\pi^*$) transition; the $S_0 \rightarrow S_2$ transition is only slightly higher in energy ($\Delta\lambda = 25$ nm). However, for the $^{5'}$G−2AP$^{3'}$ dimer, the $S_0 \rightarrow S_2$ transition has a wavelength and oscillator strength similar to those of the isolated 2AP monomer and its $S_0 \rightarrow S_1$ transition is much lower in energy ($\Delta\lambda = 56$ nm) with a smaller oscillator strength. Comparison of the dimers clearly shows the importance of the relative geometry of the bases in determining the electronic structure and nature of the excited state transitions.

The calculated excitation wavelengths and oscillator strengths of the first three singlet transitions of the $^{5'}$G−2AP−G$^{3'}$ trimer are shown in Figure 2c. The $S_0 \rightarrow S_3$ transition is moderately allowed and has a wavelength that is slightly blue-shifted from that of the isolated 2AP $\pi-\pi^*$ transition. The oscillator strength of this transition is calculated to be only ~40% of that of the isolated 2AP transition, and as a result, the radiative rate of this trimer transition is predicted to be ~(40 ns)$^{-1}$. Like that of the $^{5'}$G−2AP$^{3'}$ dimer, the trimer $S_0 \rightarrow S_1$ transition has a very low

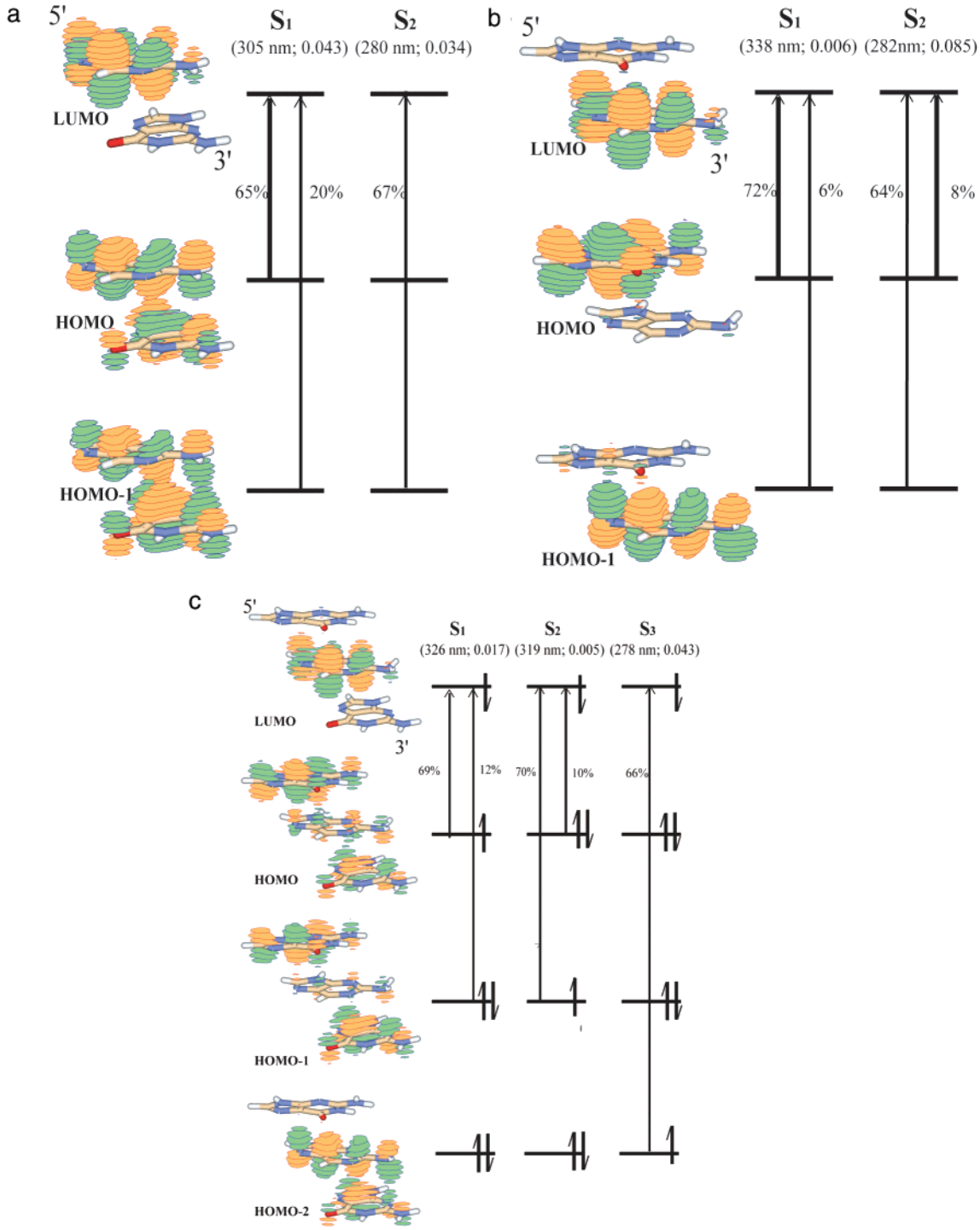

FIGURE 2: Transition wavelengths, oscillator strengths, and one-electron contributions (>10%) for the low-lying excited singlet transitions for systems with 2AP stacked with guanine: (a) $^{5'}$2AP−G$^{3'}$, (b) $^{5'}$G−2AP$^{3'}$, and (c) $^{5'}$G−2AP−G$^{3'}$. In panel c, the electron configuration for the dominant one-electron contribution to each excited state transition is shown.

oscillator strength. However, the presence of the additional guanine in the trimer gives rise to a second state (S_2), which does not correlate with an excited state of either of the 2AP−G dimers.

In the case of 2AP flanked on either side by purines, consideration of the supermolecule orbitals is essential to understanding the photophysics. What is particularly notable for these assemblies is that electron density is delocalized over all bases (dimer or trimer) in the two highest occupied orbitals (HOMO−1 and HOMO), but localized primarily on the 2AP in the lowest unoccupied orbital (LUMO). In the $^{5'}$2AP−G$^{3'}$ dimer, electron promotions from the HOMO−1 and HOMO to the LUMO (the dominant contributions to both $S_0 \rightarrow S_1$ and $S_0 \rightarrow S_2$ transitions) result in partial hole transfer (loss of electron density) to G. In this dimer, nonradiative relaxation from $S_2 \rightarrow S_1$ does not substantially change the charge distribution. However, in the $^{5'}$G−2AP$^{3'}$ dimer, the same transition results in transfer of a hole to the G. In the trimer, electron density in the occupied orbitals is delocalized over both guanines, while in the LUMO, electron density is concentrated on the 2AP. Promotion of an electron from the delocalized HOMO−2 to the LUMO produces the

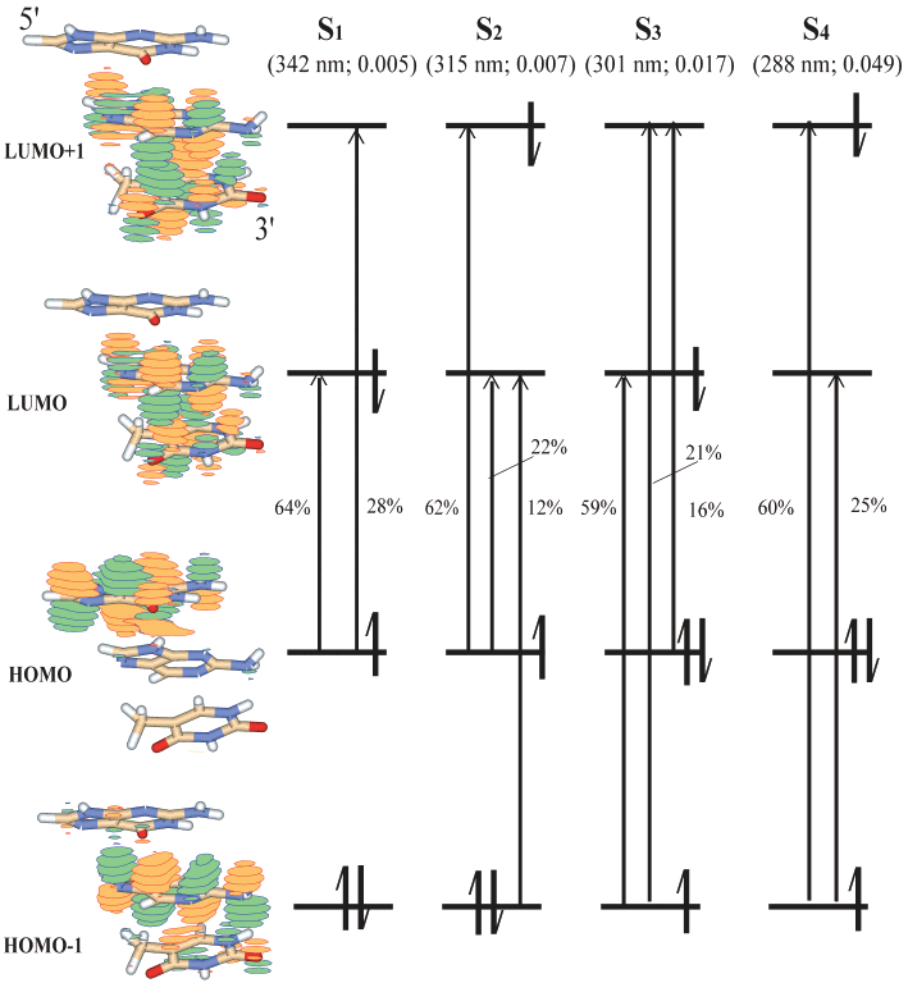

FIGURE 3: Transition wavelengths, oscillator strengths, and one-electron contributions (>10%) for the low-lying excited singlet transitions of the $^{5'}$G−2AP−T$^{3'}$ trimer. The electron configuration for the dominant one-electron contribution to each excited state transition is shown.

dominant configuration of the fluorescent S_3 state. Relaxation from S_3 to S_2 (S_1) results in partial hole transfer to both the 5′ and 3′ G. This is easily seen by examining the dominant electron configurations for the excited states, which are shown in Figure 2. An important point is that the stronger stacking interactions among the purines results in electronic transitions for the trimer that cannot be reduced to a superposition of dimer transitions.

2-Aminopurine fluorescence in this trimer would be compromised by the strong ground state interactions between the monomers leading to substantial mixing of localized and CT transitions, as well as by nonradiative transitions from the fluorescent S_3 state to the S_1 and/or S_2 state. Had the calculations been performed with adenine, rather than guanine, the results are predicted to be qualitatively similar [as seen in the $^{5'}$2AP−A$^{3'}$ dimer (*19*)], although complicating that prediction is the similarity in the ionization potentials of 2AP and adenine, which may alter the extent of mixing of the monomer HOMOs.

2-Aminopurine Flanked by Purine and Pyrimidine ($^{5'}$G−2AP−T$^{3'}$). The electronic structure of this trimer is shown in Figure 3. There are now four excited state transitions in the relevant spectral region, with the $S_0 \rightarrow S_4$ transition being the most 2AP-like on the basis of oscillator strength and transition wavelength. As was seen with the other trimers, the stacking interaction leads to a reduction of the oscillator strength of the 2AP-like transition compared to the $S_0 \rightarrow S_1$ transition of isolated 2AP. The S_3 and S_4 states derive primarily from configurations resulting from one-electron promotions from a 2AP-localized HOMO−1 to unoccupied orbitals that are delocalized over the 2AP−T fragment. The $S_0 \rightarrow S_3$ and $S_0 \rightarrow S_4$ transitions thus have partial electron transfer character (to the T). The S_2 and S_1 states, however, result from promotion from the HOMO, which is localized on the G, and are nearly pure CT states (hole transfer from the 2AP−T dimer to G).

The supermolecule MOs involved in the low-lying excited state transitions of this trimer clearly correlate with those of either the $^{5'}$G−2AP$^{3'}$ or $^{5'}$2AP−T$^{3'}$ fragment. The $^{5'}$G−2AP$^{3'}$ dimer exhibits electronic transitions that either are localized on the 2AP or have significant charge transfer character. Similarly, the $^{5'}$2AP−T$^{3'}$ dimer also leads to a CT state below a localized 2AP-like state. However, each of the dimer fragments was characterized by a localized 2AP-like S_2 state and a charge transfer S_1 state. In the trimer, there are three states below the 2AP-like state. Its $S_0 \rightarrow S_1$ and $S_0 \rightarrow S_2$ transitions involve primarily promotion of an electron out of the localized guanine orbital (HOMO) into unoccupied orbitals that are delocalized over the 2AP−T fragment. These two transitions produce a localized hole on the guanine and a delocalized negative charge over the 2AP−T dimer. The $S_0 \rightarrow S_3$ and $S_0 \rightarrow S_4$ transitions receive substantial contributions from HOMO−1 → LUMO (LUMO+1), and thus, these transitions resemble those of 2AP, although with

some charge transfer character to the 3′ thymine. The S_3 state, in particular, has components of both 2AP → G hole transfer and 2AP → T electron transfer in addition to localized 2AP character.

Nonradiative transitions from the fluorescent S_4 state to lower-lying states yield two chemically distinct relaxation pathways as is evident from the dominant electron configurations for each state. The net effect of the $S_4 \rightarrow S_3$ transition is a slight shift in electron density from the $^{5'}$G−2AP fragment to the 2AP−$T^{3'}$ fragment. Nonradiative relaxation from the S_4 to S_2 state (S_1) results in transfer of a localized hole to the G.

DISCUSSION

These new trimer results show that stacking of 2AP with other nucleobases leads to the formation of two or more excited states with substantial charge transfer character energetically below a 2AP-like transition. The computed values of the oscillator strengths for the CT transitions may contain considerable relative error due to small errors in the determination of the one-electron amplitudes. Indeed, no experimental evidence for weak transitions to the red of the 2AP transition in 2AP-labeled nucleic acids has been reported. The low oscillator strengths characteristic of CT transitions would make them difficult to detect in absorption; however, in the present case, they would play a critical role in determining the fluorescence properties of the dimers and trimers by providing nonradiative relaxation pathways for excitation deposited in the dipole-allowed 2AP-like state.

Whether the CT states are primarily hole transfer or electron transfer in character is dependent on the identity of the stacking partners. When 2AP is flanked by pyrimidines, strong mixing of unoccupied orbitals leads to low-lying states characterized by a localized 2AP hole and a delocalized electron. Stacking with purines results in the formation of occupied trimer MOs that are delocalized over all three bases and a LUMO localized on the 2AP; the excited states involve considerable hole transfer to one or both purines. When 2AP is flanked by both guanine and thymine, both hole and electron transfer states result. These *in silico* calculations support the interpretation of in vitro transient absorption studies of Barton, Zewail, and co-workers on 2AP-labeled DNA duplexes, based on the sequence dependence of the excited state lifetime (*18*). Our qualitative MO analysis predicts that excitation of 2AP will be quenched by hole transfer to a neighboring guanine or by electron transfer to a neighboring thymine.

Electronic State Ordering and Vibrational Relaxation. The TDDFT results reflect the vertical transition energies for 2AP−T dimers and trimers at the geometry corresponding to the ground electronic state. Excitation into an excited state will result in rapid relaxation of the Franck−Condon active vibrations, leading to a slightly altered (relaxed) geometry for the assembly. The theory of nonradiative electronic relaxation processes relies on vibrational relaxation preceding electronic relaxation. To further establish the viability of charge transfer processes as fluorescence quenching mechanisms for 2AP in DNA, it is necessary to consider the relative energetics of the 2AP-like and CT states at the geometry corresponding to the vibrationally relaxed 2AP-like state. To do this rigorously, an energy minimization of the entire assembly is required, but is precluded with current implementations of TDDFT. To approximate the vibrationally relaxed excited state geometry, the following argument is applied to the $^{5'}$T−2AP−$T^{3'}$ trimer. Due to the localized nature of the optically accessible transition ($S_0 \rightarrow S_3$), the vibrational dynamics following excitation will primarily involve the 2AP ring system, leading to the simplification that the relaxed geometry of the excited trimer can be approximated by the optimized geometry of the 2AP monomer in its S_1 state. Previous geometry optimization of this state at the CIS/6-31G(d,p) level (*23*) showed that excitation into the $\pi-\pi^*$ state results in lengthening of the N_7-N_8 bond in the five-membered ring and distortion of the six-membered ring. As a consequence, the N_1-C_6 and C_4-C_5 bond lengths increase and C_6 is out of plane. Qualitatively similar results for the 2AP S_1 geometry have recently been obtained by Rachovsky et al. (*25*), who used the CASSCF method.

TDDFT results for the vertical transition energies from this "relaxed" trimer show that the Franck−Condon energy for the S_3 state is approximately 1300 cm^{-1} (0.16 eV). Comparison of the trimer ground state energies for the two geometries gives a value of ∼1375 cm^{-1} for the Franck−Condon energy associated with the vertical $S_3 \rightarrow S_0$ transition; thus, the fluorescence maximum is predicted to be at 318 nm. We note that the predicted Stokes shift only takes into account the structural reorganization of the 2AP and does not include reorganization of low-frequency trimer vibrational modes or solvent reorganization. More importantly, the state ordering is unaffected, which demonstrates that CT processes are energetically favorable following vibrational relaxation of the initially excited state. The CT state energies are, in fact, also lowered by vibrational relaxation of 2AP, which further demonstrates the sensitivity of these states to small changes in orbital overlap.

Quenching Mechanisms. The TDDFT results provide a detailed picture of the excited state structure of 2AP-containing assemblies. To construct a photophysical model to explain 2AP fluorescence quenching in nucleic acids, it is important to establish the nature of the emitting state.

That the fluorescence observed in time-resolved studies of 2AP-labeled DNAs arises from a localized 2AP state is clearly evident from the recent experiments of Larsen et al. (*16*). Decay-associated spectra of the ultrafast (∼10 ps) component and the long 9.8 ns component are virtually indistinguishable with peak maxima (∼370 nm) nearly identical to that of free 2AP in solution. Extrapolation of their time-resolved anisotropy [$r(t)$] measurements back to zero time delay gives values for $r(0)$ of ∼0.35, which is close to the theoretical maximum (0.40) expected for emission from the initially excited state and nearly identical to the value obtained for free 2AP. In addition, the transient absorption studies of Wan et al. on 2AP-containing DNA duplexes provide strong evidence that the state probed in their experiments is the 2AP $\pi-\pi^*$ state. Furthermore, no evidence exists for weak time-resolved emission that is more red than that of 2AP in a nucleic acid, indicating that the CT states return to the ground state (i.e., charge recombination) nonradiatively. These observations provide strong evidence that the fluorescence observed in both time-resolved and steady state experiments on 2AP-labeled DNA originates

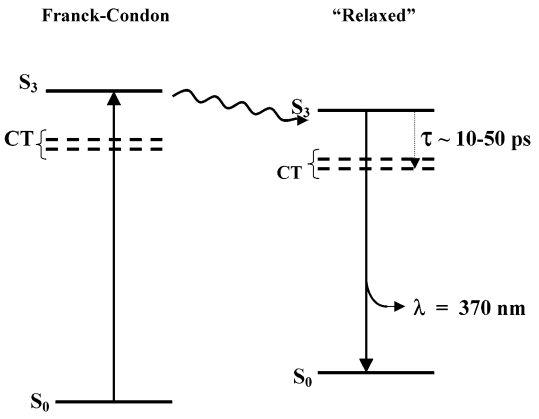

FIGURE 4: Jablonski diagram of the excitation and relaxation pathways predicted for the $^{5'}$T−2AP−T$^{3'}$ trimer. The wavy arrow denotes the vibration of the initially excited S_3 state, and the dotted arrow denotes the nonradiative electronic relaxation of the fluorescing state. The fluorescence maximum of 370 nm includes both the intramolecular and solvent contribution Stokes shift.

solely from a localized excited state that is substantially 2AP in character.

Our results, applied to those experimental observations, lead to the following picture of the excited state dynamics following photoexcitation of 2AP in a perfectly stacked (i.e., B-form) DNA, which we illustrate for the case of the $^{5'}$T−2AP−T$^{3'}$ trimer with the Jablonski diagram in Figure 4. Excitation into the 2AP-like S_3 state initiates ultrafast vibrational relaxation and solvation processes followed by nonradiative electronic relaxation to either the S_2 or S_1 state (i.e., electron transfer to either the 5′ or 3′ T). The relative rates of these two pathways cannot be determined, since we currently have no knowledge of the solvent and intermolecular reorganization energies. Knowledge of the reorganization energies and electronic coupling terms would allow the calculation of the relative rates via Marcus theory (*41*, *42*).

On the basis of our results for the state ordering and oscillator strengths of the dimers and trimers, we propose that quenching of 2AP in nucleic acids can occur by two mechanistically distinct processes. The first of these, as illustrated above, involves loss of energy from the fluorescent state via nonradiative relaxation to one or more charge transfer states, which are absent in free 2AP. This mechanism is similar to that normally termed diffusional (dynamic) quenching in that it evolves from the *excited state* of the fluorophore. In the present case, however, diffusion of the quencher to the fluorophore is obviously unnecessary. This type of quenching is reminiscent of dynamic quenching in the limit of large quencher concentration, where the quenching rate is governed by the intrinsic kinetics of the quenching process rather than by diffusion, a scenario sometimes termed "apparent static" quenching (*43*). Under conditions where $\tau_{nrad} \ll \tau_{rad}$ (normally the case for 2AP in nucleic acids), the experimentally observed lifetime [$\tau_{obs} = \tau_{nrad}\tau_{rad}/(\tau_{nrad} + \tau_{rad}) \approx \tau_{nrad}$] provides a direct measure of the charge transfer rate.

The calculations also suggest a second mechanism for reduction of the observed quantum yield for 2AP in a nucleic acid. The loss of oscillator strength of the localized 2AP transition arising from strong π-orbital overlap predicts that the quantum yield would be lowered by the proportionally reduced radiative rate. The extent to which a change in the radiative rate would influence the measured lifetime and quantum yield depends on the magnitude of the competing nonradiative rates. In the limit $\tau_{nrad} \ll \tau_{rad}$, a 10% reduction in oscillator strength would lead to an ~10% reduction in the yield, for example, but virtually no change in lifetime. Our results show that the reduction of the oscillator strength of the fluorescing transition arises in large part from the strong *ground state* interactions between 2AP and its neighbors. In this sense, it bears some similarity to "static" quenching; however, the traditional description of static quenching involves formation of a nonfluorescent ground state complex, rather than a ground state complex with altered radiative properties.

The two mechanisms described here differ in their electronic origin; ground state perturbations of the fluorophore lead to changes in its radiative rate, whereas the formation of CT states leads to enhanced excited state decay via nonradiative pathways. Both mechanisms predict changes in lifetime and steady state yield. Clearly, both lifetime and quantum yield measurements are necessary to fully characterize the quenching mechanisms operating in any given system.

We note that the presence of multiple states with CT character below the dipole-allowed 2AP-like state does not, by itself, imply nonexponential decay kinetics for the fluorescent 2AP state. If there existed an ensemble of trimers in which the static geometry of each molecule was exactly that of its neighbors, the observed nonradiative decay from the 2AP excited state would be single-exponential with a rate constant equal to the sum of the rate constants for the individual charge transfer processes. Nonexponential fluorescence decays will arise from dynamical motions that modulate the relative orientations of the bases. Fluctuations of the energy gap and/or mixing of localized and CT states on time scales similar to or longer than nonradiative decay of the 2AP state will lead to nonexponential fluorescence decays.

2-Aminopurine Dimers with Non-B-Form Geometry. The observation of nonexponential fluorescence decays in 2AP-labeled DNA has been interpreted to indicate the presence of a distribution of (partially) stacked conformations for the 2AP, each with a different decay rate (*2*). The physical origin of this distribution in double-stranded DNA is "breathing" (*44*), a dynamic process wherein the bases move away from their hydrogen-bonded positions in the duplex. In some fraction of events, breathing results in breakage of the base pair, which is manifested in NMR experiments by the exchange of guanosine and thymine imino protons with solvent (water) protons; estimates of base pair half-lives are on the order of milliseconds (*45*, *46*). For such exchange to occur, the hydrogen bonds between base pairs must be disrupted and the base(s) moved out of the normal position in the duplex to expose the imino proton to solvent. The physical extent of excursion of the base(s) is unknown; it is plausible to assume that a large excursion would be rare, while smaller excursions take place more often and on rapid time scales. Stochastic dynamics simulations support this picture (*47*).

When 2AP breathes in a duplex, or when its stacking with flanking bases in a single strand is disrupted, the resulting distortion of stacking interactions is predicted to alter the electronic structure of the supermolecule. A simple example

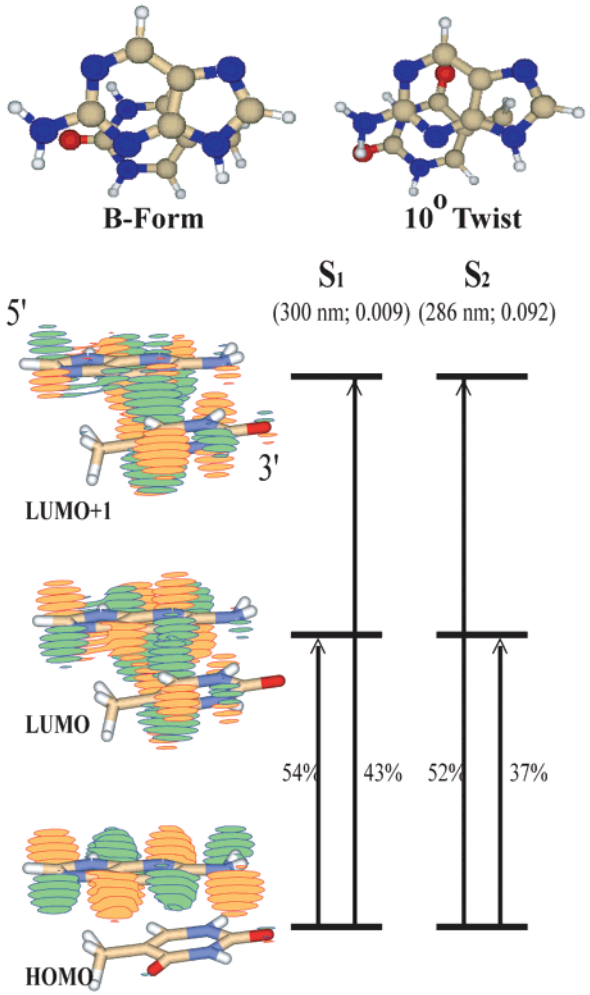

FIGURE 5: Transition wavelengths, oscillator strengths, and dominant one-electron orbital contributions (>10%) for the first two singlet transitions of a distorted $^{5'}$2AP−T$^{3'}$ dimer. The 2AP has been rotated about the ζ O3′−P backbone torsion 10° toward the major groove.

of the sensitivity of electronic structure to geometric structure was seen for 2AP dimers in which the flanking base was either 3′ or 5′. To probe for the effect of structural variations on the electronic structure of $^{5'}$2AP−T$^{3'}$ dimers, we have reduced the stacking interaction typical of adjacent bases in B-form DNA and recalculated the electronic structure for three new geometries.

Distorted $^{5'}$2AP−T$^{3'}$ dimer structures were generated by small rotations about the backbone (ζ; 2AP O$^{3'}$−P) such that the 2AP base plane remains (nearly) parallel to that of thymine at a vertical displacement of 3.4 Å, but where their base planes are twisted relative to each other by 5−15° away from the canonical B-form overlap. The O$^{3'}$−P bond vector has substantial projection onto the helical axis; thus, the primary effect is to move the 2AP toward what in a duplex would be the major groove, resulting in changes in orbital overlap. Figure 5 shows the MOs and one-electron contributions to the $S_0 \rightarrow S_1$ and $S_0 \rightarrow S_2$ transitions for a dimer in which the 2AP has been rotated 10°. Also shown are the B-form and 10° structures looking down the helical axis from the 5′ side, which clearly illustrate the effect of this motion on the overlap of the two ring systems.

Characteristics of the B-form $^{5'}$2AP−T$^{3'}$ dimers are preserved in these distorted dimers; the HOMO of the dimer

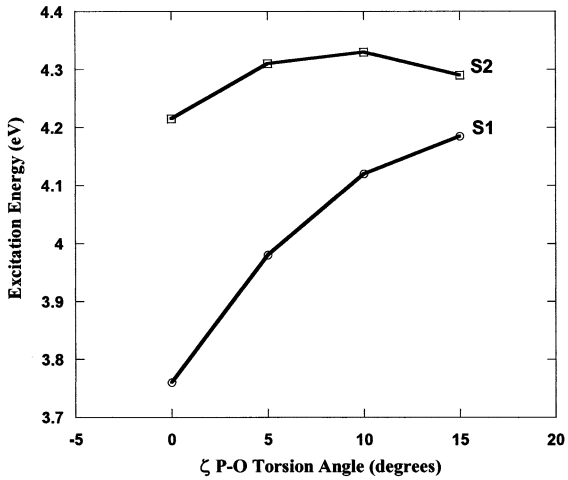

FIGURE 6: Energy as a function of rotation angle about the ζ O3′−P backbone torsion for the $S_0 \rightarrow S_1$ (CT) and $S_0 \rightarrow S_2$ (2AP) transitions of the $^{5'}$2AP−T$^{3'}$ dimer.

remains essentially purely 2AP in character, while the excited states show substantial charge transfer features (dimer LUMO and LUMO+1 remain highly delocalized). Substantial mixing of HOMOs in $^{5'}$G−G$^{3'}$ dimers over a wide range of twist angles about the helical axis has also been observed by Sugiyama and Saito (*48*). It is important to point out that neither simple rotation about the ζ torsion nor simple rotation about the helical axis represents the reaction coordinate for breathing; however, these distortions do result in partially unstacked structures that should approximate those present in solution. Unlike the B-form $^{5'}$2AP−T$^{3'}$ dimer (Figure 1a), the extent to which the monomer LUMOs mix to produce the dimer LUMO and LUMO+1 is different with electron density shared nearly equally between these two orbitals in the distorted dimer. Both $S_0 \rightarrow S_1$ and $S_0 \rightarrow S_2$ transitions receive similar contributions from the HOMO → LUMO and HOMO → LUMO+1 transitions. Despite the differences in electronic structure, the oscillator strengths of these two transitions are relatively unchanged from those of the B-form structure. Differences noted in the extent of mixing of the monomer excited orbitals are summarized by plotting the energies ($\sim\lambda^{-1}$) of the $S_0 \rightarrow S_1$ and $S_0 \rightarrow S_2$ transitions as a function of twist angle (Figure 6). As expected, the energy of the S_1 state is sensitive to the extent of base stacking, but calculations predict that quenching of the fluorescent state will still occur. The nonradiative relaxation rate from the S_2 to S_1 state will depend on the energy gap between the states. The distorted dimer model, though simplistic, does provide a qualitative explanation for the nonexponential fluorescence decays observed for 2AP in nucleic acids in terms of the influence of π-stacking on the energetic coupling of the fluorescent and CT states. The observation of highly nonexponential decays with components ranging from 10 ps to 10 ns suggests that the time scales of 2AP breathing motions (conformational changes) large enough to alter the 2AP decay rate are on the order of nanoseconds or longer.

2-Aminopurine Fluorescence Observed in Nucleic Acids. We have shown that both the sequence and conformation of bases flanking a 2AP base in a single strand of nucleic acid can dramatically affect its photophysical properties. On the basis of the electronic structure of these trimers and their substituent dimers, we propose that quenching of 2AP

fluorescence as a result of π-stacking can occur either via introduction of new nonradiative pathways involving CT states or through alteration of the absorptive properties due to electron delocalization in the ground state.

The specific contribution of each quenching mechanism to the observed steady state and time-resolved fluorescence of 2AP in a nucleic acid cannot be derived from our calculations here. These results are currently being tested by in vitro steady state and lifetime experiments in our laboratory to determine whether the observed fluorescence properties of 2AP in these trimers are as predicted.

ACKNOWLEDGMENT

J.M.J. acknowledges helpful discussions with Profs. Patrik Callis and Anders Carlsson.

REFERENCES

1. Ward, D. C., Reich, E., and Stryer, L. (1969) *J. Biol. Chem. 244*, 1228.
2. Nordlund, T. M., Andersson, S., Nilsson, L., Rigler, R., Gräslund, A., and McLaughlin, L. W. (1989) *Biochemistry 28*, 9095.
3. Nordlund, T. M., Xu, D., and Evans, K. O. (1993) *Biochemistry 32*, 12090.
4. Stivers, J. T. (1998) *Nucleic Acids Res. 26*, 3837.
5. Rachofsky, E. L., Seibert, E., Stivers, J. T., Osman, R., and Ross, J. B. A. (2001) *Biochemistry 40*, 957.
6. Guest, C. R., Hochstrasser, R. A., Sowers, L. C., and Millar, D. P. (1991) *Biochemistry 30*, 3271.
7. Menger, M., Tuschl, T., Eckstein, F., and Porschke, D. (1996) *Biochemistry 35*, 14710.
8. Bandwar, R. P., and Patel, S. S. (2001) *J. Biol. Chem. 276*, 14075.
9. Újvári, A., and Martin, C. T. (1996) *Biochemistry 35*, 14574.
10. Jia, Y., Kumar, A., and Patel, S. S. (1996) *J. Biol. Chem. 271*, 30451.
11. Allan, B. W., Reich, N. O., and Beechem, J. M. (1999) *Biochemistry 38*, 5308.
12. Beechem, J. M., Otto, M. R., Bloom, L. B., Eritja, R., Reha-Krantz, L. J., and Goodman, M. F. (1998) *Biochemistry 37*, 10144.
13. Raney, K. D., Sowers, L. C., Millar, D. P., and Benkovic, S. J. (1994) *Proc. Natl. Acad. Sci. U.S.A. 91*, 6644.
14. Holz, B., Klimasauskas, S., Serva, S., and Weinhold, E. (1998) *Nucleic Acids Res. 26*, 1076.
15. Baliga, R., Baird, E. E., Herman, D. M., Melander, C., Dervan, P. B., and Crothers, D. M. (2001) *Biochemistry 40*, 3.
16. Larsen, O. F. A., van Stokkum, I. H. M., Gobets, B., van Grondelle, R., and vanAmerongen, H. (2001) *Biophys. J. 81*, 1115.
17. Kelley, S. O., and Barton, J. K. (1999) *Science 283*, 375.
18. Wan, C., Fiebig, T., Schiemann, O., Barton, J. K., and Zewail, A. H. (2000) *Proc. Natl. Acad. Sci. U.S.A. 97*, 14052.
19. Jean, J. M., and Hall, K. B. (2001) *Proc. Natl. Acad. Sci. U.S.A. 98*, 37.
20. Rachofsky, E. L., Osman, R., and Ross, J. B. A. (2001) *Biochemistry 40*, 946.
21. Broo, A. (1998) *J. Phys. Chem. A 102*, 526.
22. Rachofsky, E. L., Ross, J. B. A., Krauss, M., and Osman, R. (1998) *Acta Phys. Pol., A 94*, 735.
23. Jean, J. M., and Hall, K. B. (2000) *J. Phys. Chem. A 104*, 1930.
24. Holmén, A., Nordén, B., and Albinsson, B. (1997) *J. Am. Chem. Soc. 119*, 3114.
25. Rachofsky, E. L., Ross, J. B. A., Krauss, M., and Osman, R. (2001) *J. Phys. Chem. A 105*, 190.
26. Parr, R. G., and Yang, W. (1989) *Density Functional Theory of Atoms and Molecules*, Oxford University Press, New York.
27. Baerends, E. J., and Gritsenko, O. V. (1997) *J. Phys. Chem. A 101*, 5383.
28. Casida, M. (1995) in *Recent Advances in Density Functional Methods* (Chong, D. P., Ed.) World Scientific, Singapore.
29. Petersilka, M., Gossmann, U. J., and Gross, E. K. U. (1996) *Phys. Rev. Lett. 76*, 1212.
30. Stratmann, R. E., Scuseria, G. E., and Frisch, M. J. (1998) *J. Chem. Phys. 109*, 8218.
31. Frisch, M. J., Trucks, G. W., Schlegel, H. B., Scuseria, G. E., Robb, M. A., Cheeseman, J. R., Zakrzewski, V. G., Montgomery, J. A., Jr., Stratmann, R. E., Burant, J. C., Dapprich, S., Millam, J. M., Daniels, A. D., Kudin, K. N., Strain, M. C., Farkas, O., Tomasi, J., Barone, V., Cossi, M., Cammi, R., Mennucci, B., Pomelli, C., Adamo, C., Clifford, S., Ochterski, J., Petersson, G. A., Ayala, P. Y., Cui, Q., Morokuma, K., Malick, D. K., Rabuck, A. D., Raghavachari, K., Foresman, J. B., Cioslowski, J., Ortiz, J. V., Stefanov, B. B., Liu, G., Liashenko, A., Piskorz, P., Komaromi, I., Gomperts, R., Martin, R. L., Fox, D. J., Keith, T., Al-Laham, M. A., Peng, C. Y., Nanayakkara, A., Gonzalez, C., Challacombe, M., Gill, P. M. W., Johnson, B. G., Chen, W., Wong, M. W., Andres, J. L., Head-Gordon, M., Replogle, E. S., and Pople, J. A. (1998) *Gaussian 98*, Gaussian, Inc., Pittsburgh, PA.
32. Schaftenaar, G., and Noordik, J. H. (2000) *J. Comput.-Aided Mol. Des. 14*, 123.
33. Becke, A. D. (1993) *J. Chem. Phys. 98*, 5648.
34. Bauernschmitt, R., and Ahlrichs, R. (1996) *Chem. Phys. Lett. 256*, 454.
35. Hsu, C.-P., So, H., and Head-Gordon, M. (2001) *J. Phys. Chem. 105*, 451.
36. Ruiz, E., Salahub, D. R., and Vela, A. (1996) *J. Phys. Chem. 100*, 12265.
37. *INSIGHT II* (1997) Molecular Simulations, Inc., San Diego.
38. Boys, S. F., and Bernardi, F. (1970) *Mol. Phys. 19*, 553.
39. Thompson, M. A., Zerner, M., and Fajer, J. (1991) *J. Phys. Chem. 95*, 5693.
40. Ricciardi, G., Rosa, A., van Gisbergen, S. J. A., and Baerends, E. J. (2000) *J. Phys. Chem. A. 104*, 635.
41. Marcus, R. A., and Sutin, N. (1985) *Biochim. Biophys. Acta 811*, 265.
42. Tavernier, H. L., and Fayer, M. D. (2000) *J. Phys. Chem. B 104*, 11541.
43. Lakowicz, J. R. (1999) *Principles of Fluorescence Spectroscopy*, 2nd ed., Kluwer/Plenum, New York.
44. Englander, S. W., and Kallenbach, N. R. (1982) *Q. Rev. Biophys. 16*, 521.
45. Guéron, M., Kochoyan, M., and Leroy, J.-L. (1987) *Nature 328*, 89.
46. Snoussi, K., and Leroy, J.-L. (2001) *Biochemistry 40*, 8898.
47. Briki, F., Ramstein, J., Lavery, R., and Genest, D. (1991) *J. Am. Chem. Soc. 113*, 2490.
48. Sugiyama, H., and Saito, I. (1996) *J. Am. Chem. Soc. 118*, 7063.

BI020308Y